CHEMISTRY

Designing high-performance hypergolic propellants based on materials genome

Wen-Li Yuan[1], Lei Zhang[1], Guo-Hong Tao[1], Shuang-Long Wang[1], You Wang[1], Qiu-Hong Zhu[1], Guo-Hao Zhang[1], Zhang Zhang[1], Ying Xue[1], Song Qin[1], Ling He[1]*, Jean'ne M. Shreeve[2]*

A new generation of rocket propellants for deep space exploration, ionic liquid propellants, with long endurance and high stability, is attracting more and more attention. However, a major defect of ionic liquid propellants that restricts their application is the inadequate hypergolic reactivity between the fuel and the oxidant, and this defect results in local burnout and accidental explosions during the launch process. We propose a visualization model to show the features of structure, density, thermal stability, and hypergolic activity for estimating propellant performances and their application abilities. This propellant materials genome and visualization model greatly improves the efficiency and quality of developing high-performance propellants, which benefits the discovery of new advanced functional molecules in the field of energetic materials.

INTRODUCTION

Since ancient times, human beings have been unwilling to confine themselves to Earth itself. For thousands of years, exploring high altitudes and space has been an unattainable and unmanageable activity relying on primitive technology. With the development of modern technology, high-performance spacecraft that can achieve space navigation has attracted much attention (*1*). As the power source of rocket or spacecraft, chemical energy released by a propellant determines the altitude, range, and service life of spacecraft (*2*), among which the high specific impulse fuel/oxidizer is one of the desirable choices for deep space exploration of rockets. For instance, the Atlas-Centaur rocket (liquid H_2/O_2, to Mars and Venus) and the Long March 3B rocket [UDMH (unsymmetric dimethyl hydrazine)/N_2O_4, to the moon]. (*3*, *4*) However, some of the high-performance rocket propellants have shortcomings such as highly toxic and decomposable fuels, viz., UDMH, or that they can only exist at an extremely low temperature of liquid H_2 (*5*). Serious accidents have happened over the history of spaceflight (*6*), causing severe pollution and billions of dollars in losses (*7*). With the prominence of environmental pollution and pursuits of the aircrafts' security, conceivable threats posed by toxicity and instability of propellants need to be eliminated as much as possible.

In the past decades, a battery composed of new materials was developed to replace current fuels. Ionic liquids, low–melting point salts with low volatility and high designability, have attracted wide attention including as energetic materials (*8*–*9*). Since dicyanamide (DCA) ionic liquids were used as spontaneously ignitable fuels (*10*), series of new structures have been reported for hypergolic ionic liquids (*11*–*12*). In general, a short ignition delay time for hypergolic propellants is an absolute necessity. Although DCA ionic liquids do not have short ignition delay times, their low toxicity, low viscosity, and high thermal stability satisfy many requirements of green rocket propellants (*13*). With the purpose of improving the ignition behavior of DCA ionic liquids, a series of hypergolic additives, including graphene, graphene oxide, and boron particulates, were tested and reported (*14*–*15*). The high carbon content of fuels produces smoke upon combustion, and high boron loadings are more prone to aggregation (*16*). Even though borane additives can form homogeneous mixtures, some of them are harmful and unstable and may decompose in the presence of air (*17*). Ideally, the best hypergolic additives are expected to have the ignition properties of hydrazine and the stability of DCA ionic liquids. In most cases, these two important properties cannot be satisfied simultaneously. Owing to a high possibility of combination for hypergolic structures, the existing research routes rely on the experience of researchers and are unable to cope with the challenge in a short time. Therefore, an efficient and systematic method for designing high-performance hypergolic additives is urgently needed.

Recently, a novel research method based on materials genomes has brought a revolutionary breakthrough in discovery of new materials (*18*). This strategy is based on a big data analysis of structures and properties of target materials and illustrated in Fig. 1. By constructing artificial intelligence programs and setting screening indices, a large number of possible structures can be analyzed systematically in a short time. Thus, a series of high-performance materials with expected properties are predicted and found successfully. The materials genome method can reduce the research period and the difficulty for developing new materials, which has been widely acknowledged in solar cell and metal-organic frameworks. (*19*–*20*) This fascinating method is also encouraging in the progress of developing propellants. In this work, we have applied the materials genome method to screen and predict the most probable structures of hypergolic additives in an innovative way.

RESULTS

Identifying the key structures of hypergolic compounds and exploring their structure-activity relationships are requisite for establishing a hypergolic materials genome database. A hypergolic reaction is an exothermic redox reaction that components spontaneously ignite when they come into contact in a rocket combustor. Many hypergolic propellants are organic compounds made up of gas-generated elements including hydrogen (H), carbon (C), and nitrogen (N). Like the relationship of gene and its base pair, the diversity of the arrangement of H, C, N, and other elements constitutes a series of hypergolic functional groups and frameworks, generating large

[1]College of Chemistry, Sichuan University, Chengdu 610064, China. [2]Department of Chemistry, University of Idaho, Moscow, ID 83844-2343, USA.
*Corresponding author. Email: lhe@scu.edu.cn (L.H.); jshreeve@uidaho.edu (J.M.S.)

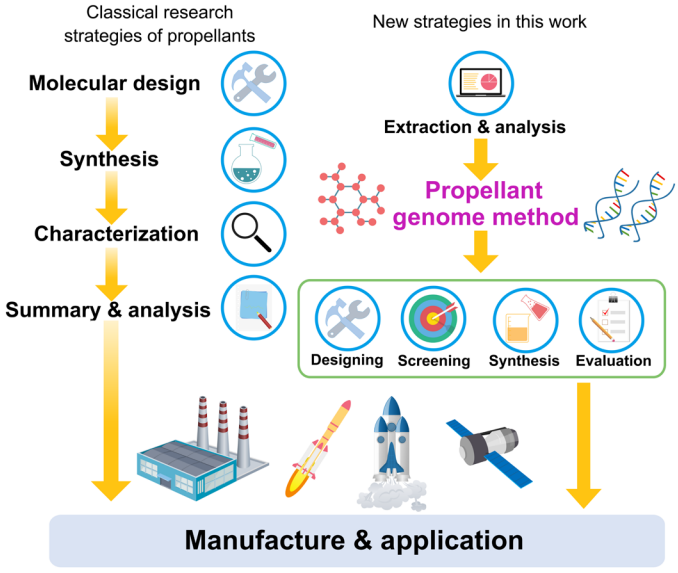

Fig. 1. New strategy in designing propellant based on genome method.

amounts of hypergolic compounds. Nevertheless, only a small proportion of hypergolic compounds are suitable for rocket propellants. In addition to the ignition delay time, a high enthalpy of combustion and a high specific impulse are also necessary. All the above aspects determine the total energy and the payload capacity of rockets (*21*). For propellant additives, more requirements also must be satisfied including good compatibility and stability. On the basis of the above analysis, we provide an objective and direct method for identifying key structures of hypergolic additives from the elemental composition and their functional structures, respectively.

The advent and use of nitrogen-rich energetic propellants can boost energy further than traditional fuels, which obviously improve the specific impulse of rocket fuels. By studying more than 1000 propellants and their mixtures found in the current literatures, relationships between their elemental composition and thermal decomposition properties were found. Statistical results show that higher nitrogen content in propellants leads to higher specific impulse (from blue to red in Fig. 2A). A propellant that contains greater than 44% nitrogen displays a specific impulse higher than 200 s, which is superior to that of conventional UDMH (198 s) and BmimDCA (187 s) (*22*, *23*). On the contrary, higher nitrogen content leads to a decrease in thermal stability in nitrogen-rich propellants. Furthermore, propellants with 30 to 50% nitrogen content have the highest thermal stability exhibiting decomposition temperatures in excess of 200°C (Fig. 2C). BmimDCA, which contains 34.1% nitrogen, is one of the most stable hypergolic propellants with decomposition occurring at 300°C. It is worth noting that the density of a propellant increases with nitrogen content increase, viz., the average value ranges from 0.91 g/cm^3 with 10% nitrogen content to 1.65 g/cm^3 with 90% nitrogen content (Fig. 2C). Considering the above requirements, an appropriate nitrogen content in the 44 to 50% range meets the specific impulse and thermal stability values required for high-performance propellants.

To provide enough chemical energy to overcome gravity, the carbon element content must generate substantial amounts of combustion heat and gaseous CO_2 necessary for spacecraft propulsion (*24*). The enthalpy of combustion relationship between carbon and nitrogen in propellants is shown in Fig. 2B. It is clear that the enthalpy of combustion of propellants is related positively to the carbon content. Although alkane propellants provide heat (48.5 kJ/g) for combustion, high–carbon content structures do not promote hypergolic ignition with oxidants. Other compounds containing more than 46% carbon would largely exhibit a more desirable combustion enthalpy than current MMH (monomethylhydrazine) and UDMH propellants (red dashed in Fig. 2D). Combining the limitation of nitrogen element in designed propellants, the carbon content range 46 to 50% is the highest allowable to achieve the best performance for specific impulse and combustion enthalpy. This is the second feature to screen target molecules.

The third feature for high-performance propellants is structural composition, which determines the stability, ignition behavior, and biological toxicity. The structural composition can be considered as two parts: framework and functional groups. Ionic liquids, which are composed of cations and anions, have unique advantages of miscibility, volatility, hypotoxicity, and thermal stability and can greatly reduce the risk of operator exposure to aerosols and deflagration (*25*). For millions of combinations of ions in ionic liquids, azole-based five-membered heterocycles anions are important sources and have a wide range of applications due to their structural adjustability and mature synthetic routes (*26*). The composition of functional groups in propellants also influences the ignition delay time. Droplet tests show that the electron-rich groups including cyano (NC^-), amino (NH_2^-), hydrazinyl ($N_2H_3^-$), and methylhydrazinyl ($CH_6N_2^-$) groups are more favorable in reacting with the oxidant (*27*–*28*). Combining the elemental composition properties mentioned above, all the key features of high-performance propellants have been extracted and analyzed. With the help of a screening program, this information provides basic guidance for rapid design and identification of target compounds.

Before constructing the screening program for target compounds, it is necessary to input the fragments of target molecules and calculate all the possible structures. Seven azole frameworks (pyrrole; imidazole; pyrazole; 1,2,3-triazole; 1,2,4-triazole; tetrazole; and pentazole) and four functional groups (NC^-, NH_2^-, $N_2H_3^-$, and $CH_3N_2H_3^-$) were taken into account. There are 517 possible structures that were calculated. Considering the influence of cations on ionic liquids (*29*), the low melting and easily prepared 1-butyl-3-methylimidazolium cation ($Bmim^+$) has been widely studied and preferred (*30*). In this work, 517 compounds with different carbon and nitrogen contents are shown in the plot in Fig. 2E (step 1). These compounds cover a wide range from 42 to 70% carbon content and 20 to 48% nitrogen content. Subsequently, the first filter of 44 to 50% nitrogen content is executed, and 24 alternative structures meet the requirement. Then, we screened the second filter of 46 to 50% carbon content, and 15 of the 24 compounds satisfy the above conditions. The results and structures are shown on the chart in Fig. 2E (step 2) and table S3. Thus, preliminary screening of high-performance additives has been completed. With the aim of selecting the best performance structure, other important indicators of additives including hypergolic reactivity and density also need to be considered comprehensively.

To further determine the most probable hypergolic additives, quantum analysis has been used to predict the properties of energetic materials. Molecular orbital (MO) theory is beneficial in evaluating the ignition behavior of hypergolic compounds (*31*). The energy gap between the highest occupied MO (HOMO) of the

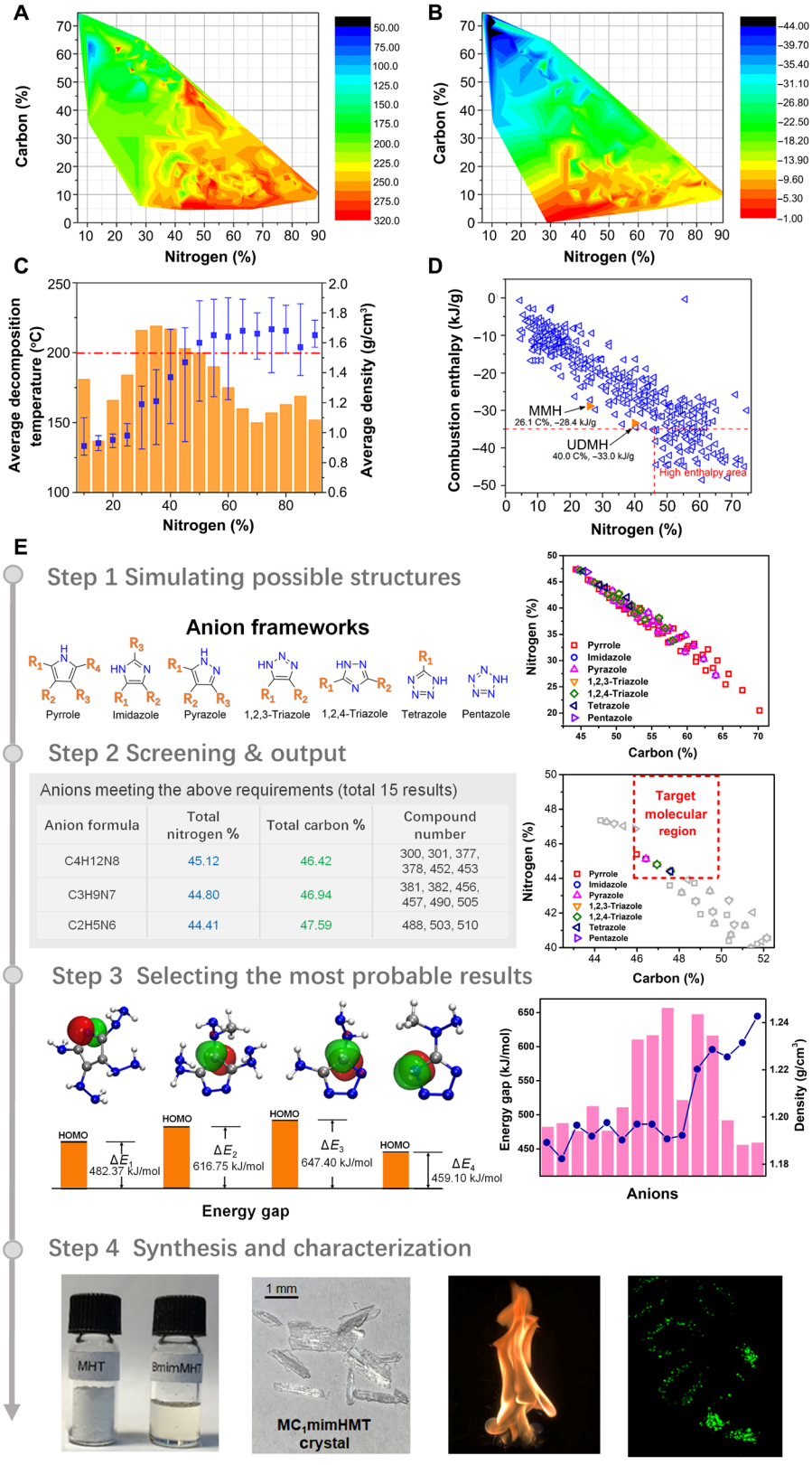

Fig. 2. Procedure of designing propellant based on materials genome. (**A** and **B**) Color-filled map of the relationships between the composition and specific impulse and between the composition and enthalpy of combustion of propellants. (**C**) Average decomposition temperature (orange histogram) and average density of propellants (blue dots) with different nitrogen content. (**D**) Relationship between carbon content and combustion enthalpy of propellants. (**E**) Steps on propellant genomic method works from theoretical speculation to experimental verification. Photo credit: Wen-Li Yuan, Sichuan University.

anions and the lowest unoccupied MO (LUMO) of HNO_3 can be explored as a criterion for the hypergolicity of the anion. Table S3 contains the energy gaps of 15 screened anions, where 4 anions have lower energy gaps, which exhibit higher reactivity in contact with oxidants, including compound no. 377, 4,5-dihydrazinyl-2-(1-methylhydrazinyl)imidazolate (DHMHI)—476.33 kJ/mol; compound no. 378, 2,5-dihydrazinyl-4-aminoimidazolate (DHAI)—476.75 kJ/mol; compound no. 505, 3,5-dihydrazinyl-1,2,4-triazolate (DHT)—456.06 kJ/mol; and compound no. 510, (1-methylhydrazinyl) tetrazolate (MHT)—459.10 kJ/mol energetic anions. In addition to reactivity with oxidants, fuel density is also of vital importance to determine the higher specific impulse and fuel loading in rockets (*32*). We further estimated the density of ionic liquids with these 15 anions, among which MHT ionic liquids have the highest density of 1.24 g/cm^3 and meet all the above requirements of hypergolic additives. As a result, the genome database and screening procedure based on high-performance hypergolic additives have been completed. To evaluate our theoretical work, we needed characterization of a series of MHT-based ionic liquids. MHT ionic liquids are prepared from neutral 5-(1-methylhydrazinyl)tetrazole, which is obtained from cyanogen azide with methylhydrazine (*33*). For further study of the structure and physicochemical properties of MHT ionic liquids, a series of imidazolium cations including 1,2,3-trimethylimidazolium (1), 1-butyl-3-methylimidazolium (2), 1-methyl-3-propargylimidazolium (3), 1-butyl-3-vinylimidazolium (4), and 1-propyl-3-vinylimidazolium (5) were synthesized successfully in good yields (85 to 90%) and fully characterized (figs. S1 and S2). The colorless crystal of 1 was characterized by single-crystal x-ray diffraction and is shown in Fig. 3. The monoclinic crystal 1 belongs to the *P*21/*c* space group with four molecules per unit cell. In the MHT anion, the N—N bond lengths of N1—N2, N2—N3, and N3—N4 in the tetrazole group are 1.356(2), 1.305(2), and 1.355(2) Å, respectively. For the composition of the methylhydrazinyl group, the N5—N6 bond 1.430(2) Å is shorter than that in neutral MMH, which can be explained by the hyperconjugation effect of tetrazole. The bond angles C1—N5—N6 116.05(15)° and C1—N5—C2 116.07(16)° are larger than that of N6—N5—C2 111.83(17)°, reflecting the steric hindrance effect of the tetrazole bulk group. The 1,2,3-trimethylimidazolium cation is nearly planar. The density of crystal 1 is 1.309 g/cm^3, with no residual solvents or disorder.

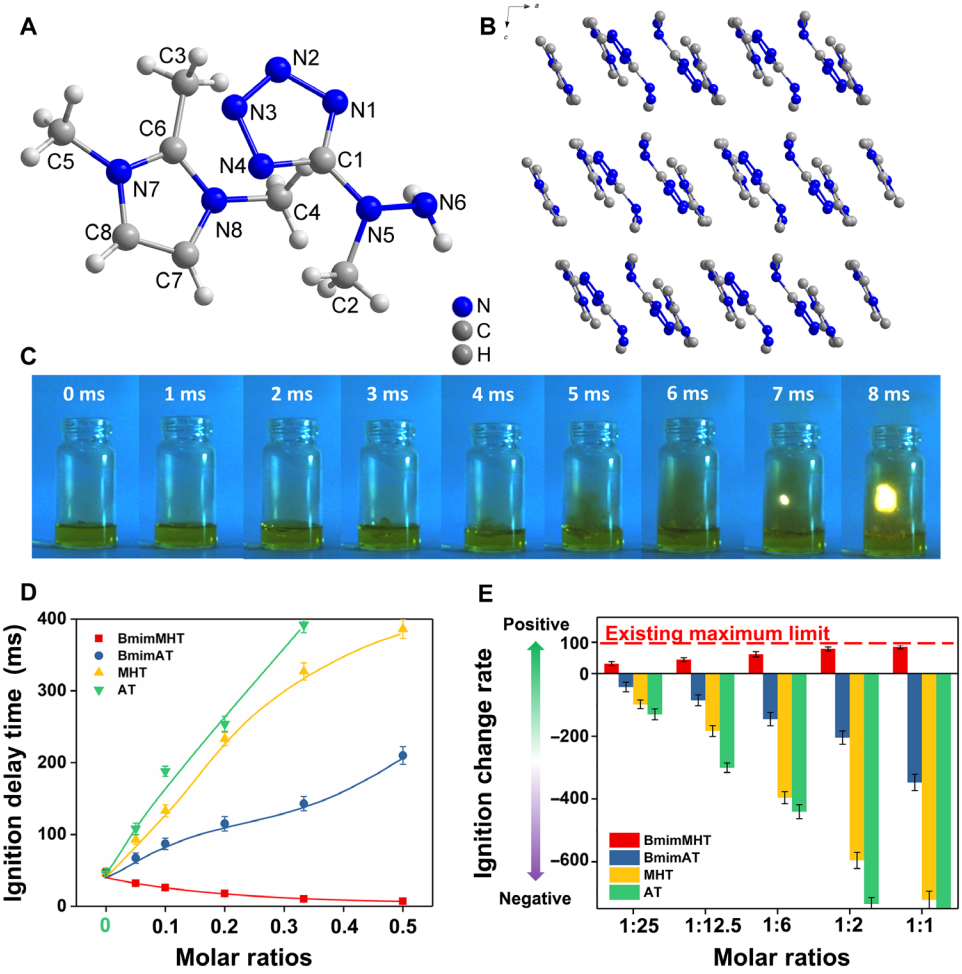

Fig. 3. Structure and hypergolic characterization of MHT ionic liquids. (**A**) Thermal ellipsoid plot (50%) of 1,2,3-trimethylimidazolium 5-(1-methylhydrazinyl) tetrazolate (1). (**B**) Packing diagram of 1 viewed down the crystallographic *b* axis. (**C**) Droplet test performed on 1:1 BmimMHT/BmimDCA solution recorded by a high-speed camera. (**D** and **E**) Ignition delay time and change ratio of BmimMHT and analogs with series molar ratio of BmimDCA ionic liquids (H atoms in crystal are omitted for clarity). Photo credit: Wen-Li Yuan, Sichuan University.

The thermal stability and detonation properties of MHT ionic liquids were studied (Table 1). All the MHT compounds are liquids at room temperature. The liquid range is larger than 170°C. Compared with UDMH at 0.79 g/cm^3 and BmimDCA at 1.06 g/cm^3, MHT ionic liquids exhibit densities that are considerably higher than 1.22 g/cm^3 (Table 1). This result is consistent with previous theoretical predictions of density. The heats of formation of MHT ionic liquids, which reflect the energy level of fuels, were also calculated and range from 424.8 to 876.1 kJ/mol, higher than the known hydrazine and BmimDCA fuels. All MHT ionic liquids are insensitive on impact and friction. BmimMHT has the highest thermal decomposition temperature of over 200°C, which would be safe under extreme conditions in space.

For evaluating the hypergolic reactivity of BmimDCA ionic liquids, a series of BmimMHT/BmimDCA ionic liquid mixtures with molar ratios from 1:25 to 1:1 were prepared and observed with a high-speed camera with white fuming nitric acid (Fig. 3C). As a result, the ignition delay time decreases as the ratio of BmimMHT/BmimDCA is increased, and a 7-ms ignition delay time was found with a molar ratio 1:1 BmimMHT/BmimDCA solution. BmimMHT as a particle-free hypergolic additive successfully improves the hypergolic reactivity of DCA ionic liquids. Nevertheless, it does not mean that the entire work of hypergolic improving program based on materials genome method has been finished. More important work to verify the repeatability and uniqueness of the experimental results is required to objectively evaluate the rationality of propellant materials genome method.

To achieve this purpose, we selected 5-(1-methylhydrazinyl)tetrazole, 5-aminotetrazole, and BmimAT as BmimMHT analogs for droplet tests. On the one hand, BmimAT, 5-(1-methylhydrazinyl)tetrazole, and 5-aminotetrazole belong to nitrogen-rich materials (*34*). The only difference is the substituted group or existing forms. On the other hand, all of them do not have the properties of high-performance hypergolic liquids mentioned before. Droplet results show that the ignition delay (ID) times of the DCA ionic liquid mixtures increased as the molar ratios of 5-(1-methylhydrazinyl)tetrazole, 5-aminotetrazole, and BmimAT rise. For molar ratio 1:1 of BmimDCA/5-aminotetrazole mixture, no hypergolic reaction was recorded. The ratio chart of additives for ignition delay time is plotted in Fig. 3E. In this chart, BmimMHT is the only one that has positive promotion in the hypergolic process. In contrast, the ID time of other samples with the 1:1 molar ratio is more than three times longer than that of pure BmimDCA. BmimMHT has become the first residue-free additive for improving hypergolic ability of BmimDCA fuels, which was designed by propellant materials genome innovatively.

By means of quantum chemistry, the mechanism of the hypergolic fuel in the ignition process can be studied systematically (*35*). Hydrogen transfer from oxidant to propellants is an important transition state during the ignition process (*36*). Investigation of electrostatic potential (ESP) on the molecular van der Waals (vdW) surface is beneficial for understanding hypergolic ignition because lower ESP values are more prototropic and lower the energy barrier of the intermediate transition state(*35*, *37*). The ESP-mapped vdW surface of BmimMHT, BmimAT, 5-(1-methylhydrazinyl)tetrazole, and 5-aminotetrazole is shown in Fig. 4A. The histogram of Fig. 4B shows the area and range of the absolute value in the molecular ESP, and percentages in different ESP areas are plotted as in Fig. 4C. Results show that BmimMHT has a global ESP minimum on the surface at −112.88 kcal/mol, lower than that of BmimAT (−104.64 kcal/mol), 5-(1-methylhydrazinyl)tetrazole (−33.06 kcal/mol), 5-aminotetrazole (−36.28 kcal/mol), and BmimDCA (−109.17 kcal/mol) (fig. S5). In terms of the negative area in BmimMHT, 19.41 Å^2 (6.92%) of the vdW surface is lower than −60 kcal/mol. For other compounds, an obvious difference in 5-aminotetrazole and 5-(1-methylhydrazinyl) tetrazole is centralized ESP charge distribution, with no area lower than −50 kcal/mol or higher than 60 kcal/mol. The negative areas below −60 kcal/mol of BmimAT and BmimDCA are 15.01 Å^2 (3.83%) and 14.06 Å^2 (5.52%), respectively, which are smaller than that of BmimMHT. This result is attributed to the MHT^- ion with a large volume and surface area. From the view of negative proportion for accepting the HNO_3 proton, the sequence of hypergolic reactivity can be estimated in BmimMHT > BmimDCA > BmimAT > 5-(1-methylhydrazinyl)tetrazole ≈ 5-aminotetrazole, which is in good agreement with the experimental observations of the droplet test.

Toxicity is always a serious problem in propellants because highly toxic hydrazine derivatives are harmful to the environment and the human body in case of leaks. However, improving high-performance hypergolic fuels without sacrificing environmental friendliness is also our purpose in this work. The toxicities of BmimMHT, BmimMHT/BmimDCA ionic liquids, and MMH were tested by the bacterium *Vibrio fischeri*, a bacterium that can determine the environmental acceptability and the toxicological parameter EC_{50} (median effective concentration). The EC_{50} results are shown in Fig. 5A. The EC_{50} of

Table 1. Physicochemical properties of MHT ionic liquids 1 to 5 and known reference compounds UDMH and BmimDCA.

Sample	ρ*	T_g†	T_d‡	$-\Delta_c H°$§	$-\Delta_f H°$‖	P¶	D#	IS**	FS††
1	1.31	−56	190	4999.8	434.9	17.44	7.02	>60	>360
2	1.23	−49	201	6368.6	424.8	15.33	6.72	>60	>360
3	1.25	−63	148	4778.7	763.7	21.18	7.87	>60	>360
4	1.22	−57	178	6649.3	537.6	16.68	7.05	>60	>360
5	1.24	−50	120	5059.8	876.1	22.31	8.10	>60	>360
UDMH‡‡	0.79	–	64	1980.1	48.3	–	–	–	–
BmimDCA§§	1.06	−6	300	6285	206.2	–	–	–	–

*Density, g/cm (25°C). †Melting point, °C. ‡Decomposition temperature, °C. §Heat of combustion, kJ/mol. ‖Heat of formation, kJ/mol. ¶Detonation pressure, GPa. #Detonation velocity, km/s. **Impact sensitivity, J. ††Friction sensitivity, N. ‡‡(*26*). §§(*27*).

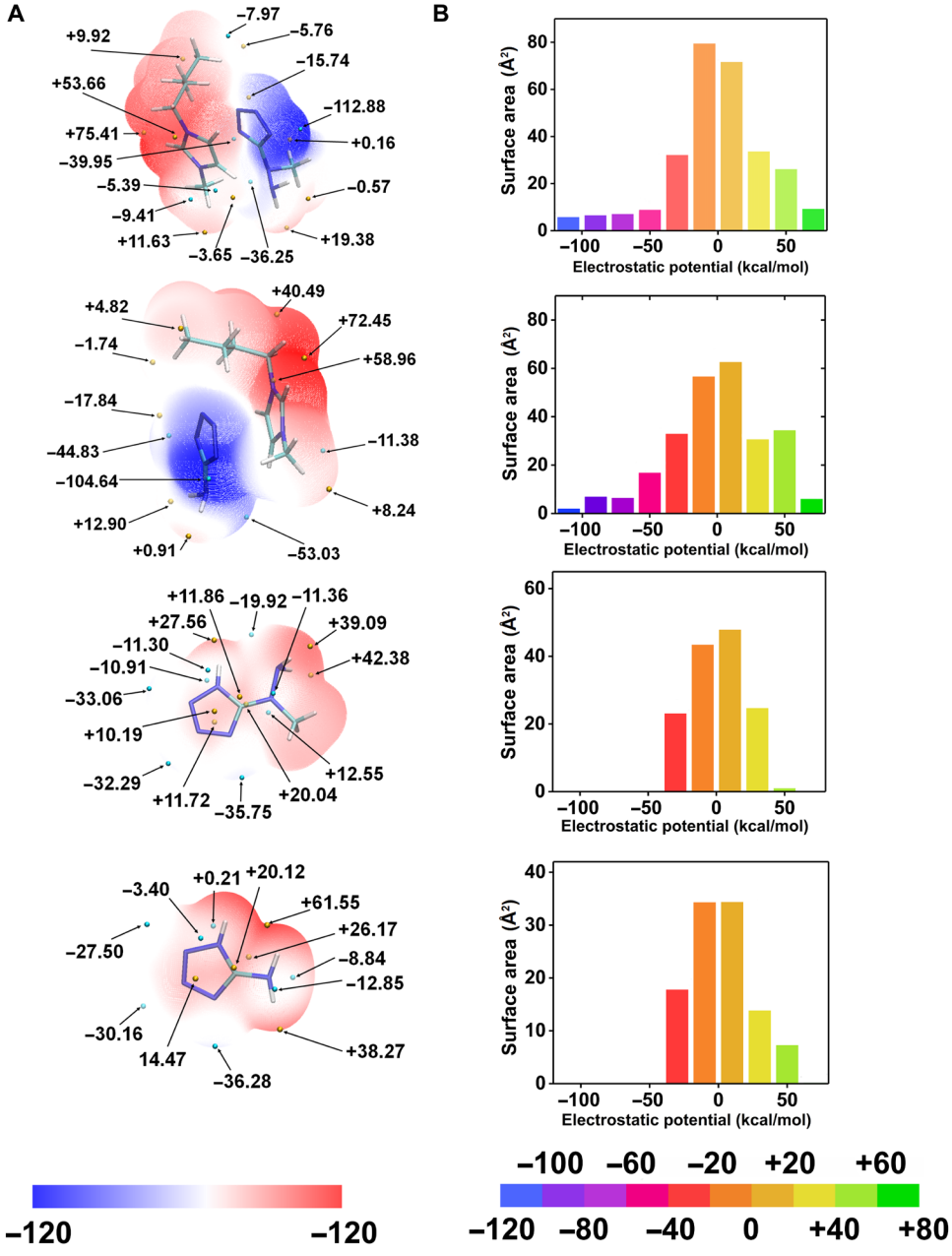

Fig. 4. ESP analysis of BmimMHT, BmimAT, MHT, and AT. (**A**) ESP-mapped molecular vdW surface of molecules with structural optimization. The units are in kilocalories per mole. The surface local minima and maxima of ESP are represented as blue and yellow points, respectively. (**B**) Surface area on vdW surface in each ESP range.

BmimMHT is 135.8 mg/liter, which exhibits lower toxicity than that of MMH (31 mg/liter), hydrazine (320 μg/liter), and UDMH (17 mg/liter) reported in the literature (*38*). In addition, the mixture of 1:1 BmimMHT/BmimDCA ionic liquid with the shortest ignition delay time shows much lower toxicity of 851.4 mg/liter in EC_{50}, and it is comparable with neat BmimDCA of 966.24 mg/liter that is recognized as an environmentally friendly ionic liquid (*39*). The BmimMHT/BmimDCA ionic liquids have more advantages as green propellants than traditional hydrazine and kerosene fuels.

Despite much other work that focuses on improving a certain performance of propellants such as combustion or ignition delay properties, in fact, whether a propellant can move to its application is determined by its combined behavior, not a single, specific indicator. This comprehensive evaluation method needs a more intuitive and accurate visualization and effectively shows the advantages and disadvantages of different propellants. In this work, we first attempted to evaluate propellants based on stability, volatility, toxicity, energetic density, and hypergolic behavior (Fig. 5B). These indicators are closely related to the production, storage, and transportation of propellants or the manufacturing of rocket fuel bunkers and engines. Relevant evaluation processes and results are given in tables S4 and S5. The ideal propellant has excellent performance in the above aspects and has the largest area in the display of radar maps. Common hydrocarbon propellants, despite exhibit considerable

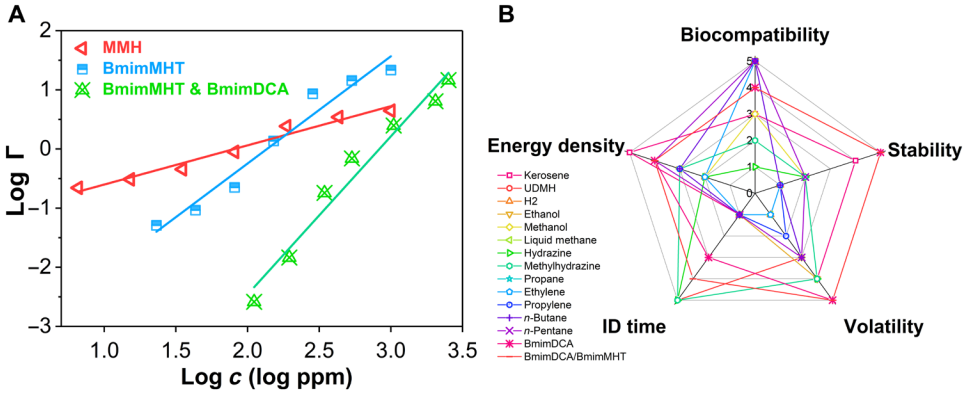

Fig. 5. Toxicity and comprehensive evaluation of ionic liquids. (**A**) Luminescent bacteria inhibition test of MMH, BmimMHT, and BmimMHT/BmimDCA with molar ratio 1:1.5. ppm, parts per million. (**B**) Evaluation results of common liquid propellants and BmimMHT/BmimDCA in this work.

biocompatibility and higher energy density for long-chain kerosene, the weak vdW force result in low boiling point, and many of them are compressed in fuel tank under low temperatures. Besides, inert hypergolicity of hydrocarbon fuels is also an intractable faultiness, which are the same as biocompatible methanol and ethanol propellants and difficult to modify or ameliorate by chemical methods (*40*). The most prominent advantage of hydrazine propellants is low ignition delay time. But the biocompatibility and stability limit the use of hydrazine fuels. In contrast, DCA ionic liquids inherit the more unique properties for ionic liquids in toxicity, stability, and volatility, which are different from molecular propellants. By virtue of the designable task-specific ionic liquids, the insufficiency of the hypergolic behavior of DCA ionic liquids has been made up by combination with BmimMHT with the guidance of the material genomic method of propellants. This previously unidentified ionic liquid propellant nearly meets all the desirable indicators and is more practical than conventional propellants, which are currently used.

DISCUSSION

In summary, we designed a previously unknown family of high-performance propellant based on propellant materials genome. The (5-methylhydrazinyl)tetrazolate ionic liquids have successfully solved the ignition behavior of DCA ionic liquids. This design strategy is beneficial for systematically summarizing the structure-activity relationship of propellants combined with the stability, ignition characteristics, and toxicity and directly gives exact results. It is the first time that the materials genome method has been introduced into the field of propellants, and this genome approach plays a guiding and promoting role in the molecular design and application of new propellants, which not only identifies residue-free green additives but also opens a new avenue to develop new high-performance propellants by expanding this approach to multiple precision forecasting.

MATERIALS AND METHODS

Synthesis of 5-(1-methylhydrazinyl)tetrazole

Sodium azide (6.5 g, 100 mmol) was added to dry acetonitrile solution of cyanogen bromide (2.0 g, 19 mmol) at 0°C. The reaction mixture was stirred for 4 hours at 0°C. After the reaction, the white precipitate was filtered with a general filtration method under atmospheric pressure. The resulting cyanogen azide solution was then added to an acetonitrile solution of methylhydrazine (300 mg, 6.5 mmol). The resulting acetonitrile solution was concentrated and dried to yield the desired product as a white powder. Yield: white solid (476 mg, 64%).

Synthesis of 1,2,3-trimethylimidazolium 5-(1-methylhydrazinyl)tetrazolate (1)

1,2,3-Trimethylimidazolium iodide (714 mg, 3.0 mmol) was dissolved in methanol, and AgMHT (994 mg, 4.5 mmol) was then added. The resulting mixture was stirred in the dark for 24 hours. Insoluble excess AgMHT along with the by-product silver iodide were removed. The filtrate was collected and dried to yield 1 as a white solid (662 mg, 92%). Clear colorless plate crystals of product suitable for x-ray structure determination were obtained after recrystallization. 1H nuclear magnetic resonance (NMR) [400 MHz, d_6-dimethyl sulfoxide (DMSO)]: δ = 7.59 (s, 2H), 4.42 (s, 2H), 3.74 (s, 6H), 2.90 (s, 3H), and 2.54 (s, 3H) parts per million (ppm). ^{13}C NMR (100 MHz, d_6-DMSO): δ = 170.02, 144.77, 121.97, 44.06, 34.69, and 9.14 ppm. Infrared (IR): ν = 3331 (m), 3137 (m), 3102 (s), 3016 (m), 2959 (s), 1623 (m), 1593 (s), 1546 (s), 1513 (vs), 1446 (s), 1406 (s), 1331 (vs), 1245 (m), 1131 (m), 1064 (s), 1042 (m), 1003 (m), 893 (v), 828 (v), 770 (m), 736 (s), 655 (vs), 586 (v), 520 (m), and 480 (m) cm^{-1}. Elemental analysis calculated (%) for C8H16N8 (224.27): C 42.84, H 7.19, N 49.96; found: C 42.79, H 7.29, N 49.92.

Synthesis of 1-butyl-3-methylimidazolium 5-(1-methylhydrazinyl)tetrazolate (2)

Using a procedure similar to that described for 1, 1-butyl-3-methylimidazolium bromide (657 mg, 3.0 mmol) and AgMHT (994 mg, 4.5 mmol) were reacted in methanol to obtain a colorless liquid (719 mg, 90%). ^{1}H NMR (400 MHz, d_6-DMSO): δ = 9.19 (s, 1H), 7.79 (s, 1H), 7.72 (s, 1H), 4.44 (s, 2H), 4.16 (t, J = 7.2 Hz, 2H), 3.85 (s, 3H), 2.90 (s, 3H), 1.75 (m, 2H), 1.24 (m, 2H), and 0.89 (t, J = 7.4 Hz, 3H) ppm. ^{13}C NMR (100 MHz, d_6-DMSO): δ = 170.50, 136.64, 123.65, 122.31, 48.50, 44.16, 35.75, 31.40, 18.80, and 13.31 ppm. IR: ν = 3314 (m), 3148 (m), 3094 (s), 2959 (s), 2936 (s), 2874 (m), 1624 (m), 1571 (s), 1496 (s), 1446 (s), 1336 (s), 1168 (s), 1126 (m), 1046 (m), 987 (m), 846 (m), 830 (m), 764 (s), 652 (vs), 622 (m), and 518 (s) cm^{-1}. Elemental analysis calculated (%) for $C_{10}H_{20}N_8$ (252.33): C 47.60, H 7.99, N 44.41; found: C 47.64, H 8.02, N 44.34.

Synthesis of 1-methyl-3-propargylimidazolium 5-(1-methylhydrazinyl)tetrazolate (3)

In a similar procedure to that described for 1, 1-methyl-3-propargylimidazolium bromide (603 mg, 3.0 mmol) and AgMHT (994 mg, 4.5 mmol) were reacted in methanol to obtain a pale yellow liquid (668 mg, 85%). ^{1}H NMR (400 MHz, d_6-DMSO): δ = 9.29 (s, 1H), 7.80 (s, 1H), 7.76 (s, 1H), 5.22 (d, J = 2.6 Hz, 2H), 4.89 (s, 3H), 3.88 (s, 3H), 3.84 (t, J = 2.6 Hz 1H), and 2.89 (s 3H) ppm. ^{13}C NMR (100 MHz, d_6-DMSO): δ = 167.52, 136.80, 124.15, 122.23, 79.00, 76.27, 43.56, 38.54, and 36.01 ppm. IR: ν = 3314 (m), 3140 (s), 3095 (s), 2962 (s), 2858 (m), 2130 (w), 1655 (m), 1575 (s), 1556 (s), 1496 (s), 1446 (s), 1334 (s), 1232 (m), 1164 (s), 1126 (m), 1084 (m), 1044 (m), 989 (m), 908 (m), 829 (s), 753 (s), 620 (s), 518 (m), and 474 (w) cm^{-1}. Elemental analysis calculated (%) for $C_9H_{14}N_8$ (234.27): C 46.14, H 6.02, N 47.83; found: C 46.04, H 6.01, N 47.95.

Synthesis of 1-butyl-3-vinylimidazolium 5-(1-methylhydrazinyl)tetrazolate (4)

With a similar procedure to that described for 1, 1-butyl-3-vinylimidazolium bromide (693 mg, 3.0 mmol) and AgMHT (994 mg, 4.5 mmol) were reacted in methanol to obtain a colorless liquid (762 mg, 96%).^{1}H NMR (400 MHz, d_6-DMSO): δ = 9.71 (s, 1H), 8.26 (s, 1H), 7.99 (s, 1H), 7.34 (dd, J = 15.7, 8.8 Hz, 1H), 5.98 (dd, J = 15.7, 2.4 Hz, 1H), 5.40 (dd, J = 8.8, 2.4 Hz, 1H), 4.50 (s, 2H), 4.22 (t, J = 7.2 Hz, 2H), 2.93 (s, 3H), 1.79 (m, 2H), 1.26 (m, 2H), and 0.87 (t, J = 7.4 Hz, 3H) ppm. ^{13}C NMR (100 MHz, d_6-DMSO): δ = 170.39, 135.61, 128.97, 123.38, 119.26, 108.60, 49.01, 44.14, 31.17, 18.87, and 13.33 ppm. IR: ν = 3322 (m), 3130 (s), 3086 (s), 3005 (m), 2961 (s), 2934 (s), 2874 (m), 1653 (s), 1571 (s), 1550 (s), 1499 (s), 1446 (s), 1338 (s), 1171 (s), 1116 (m), 1049 (m), 962 (s), 914 (s), 829 (m), 764 (s), 681 (w), 650 (m), 626 (s), 599 (s), 519 (s), and 433 (w) cm^{-1}. Elemental analysis calculated (%) for $C_{11}H_{20}N_8$ (246.34): C 49.98, H 7.63, N 42.39; found: C 50.04, H 7.66, N 42.30.

Synthesis of 1-propyl-3-vinylimidazolium 5-(1-methylhydrazinyl)tetrazolate (5)

In a similar procedure to that described for 1, 1-propyl-3-vinylimidazolium bromide (639 mg, 3.0 mmol) and AgMHT (994 mg, 4.5 mmol) were reacted in methanol to obtain a pale yellow liquid (717 mg, 89%). ^{1}H NMR (400 MHz, d_6-DMSO): δ = 9.72 (s, 1H), 8.31 (s, 1H), 7.99 (s, 1H), 7.37 (dd, J = 15.7, 8.8 Hz, 1H), 6.01 (dd, J = 15.7, 2.5, 1H), 5.43 (dd, J = 8.7, 2.4, 1H), 5.28 (d, J = 2.6 Hz, 2H), 4.91 (s, 2H), 3.90 (t, J = 2.6 Hz, 1H), and 2.94 (s, 3H) ppm. ^{13}C NMR (100 MHz, d_6-DMSO): δ = 169.22, 135.78, 128.88, 123.20, 119.45, 109.11, 79.43, 75.81, 43.93, and 39.00 ppm. IR: ν = 3134 (s), 3091 (s), 2964 (s), 2861 (m), 2129 (m), 1651 (s), 1551 (s), 1499 (s), 1444 (s), 1337 (s), 1165 (s), 1125 (m), 1106 (m), 1045 (w), 1026 (w), 957 (s), 915 (s), 829 (m), 742 (s), 659 (s), 614 (s), 597 (s), and 518 (s) cm^{-1}. Elemental analysis calculated (%) for $C_{10}H_{14}N_8$ (246.28): C 48.77, H 5.73, N 45.50; found: C 48.85, H 5.77, N 45.38.

Computational methods

Computations were performed by the Gaussian 09 (Revision A.02) suites of programs (*41*). The geometric optimization, frequency analyses, MO analyses and ESP analyses of all the compounds were carried out using Beck's three-parameter exchange function and the gradient-corrected function of Lee, Yang, Parr (B3LYP). (*42*) The standard 6-311+G(2d, p) basis set was applied for frequency analyses of structures in gas phase and characterized to be true local energy minima on the potential energy surface without imaginary frequencies (*43*). MO results are also calculated on the basis of the optimization structures in gas phase at the B3LYP/6-311+G(2d, p) level. The HOMO-LUMO gap of molecules is calculated by Multiwfn Software (version 3.6) (*44*).

SUPPLEMENTARY MATERIALS

Supplementary material for this article is available at http://advances.sciencemag.org/cgi/content/full/6/49/eabb1899/DC1

REFERENCES AND NOTES

1. E. Gibney, First private Moon lander heralds new lunar space race. *Nature* **566**, 434–436 (2019).
2. G. P. Sutton, *History of Liquid Propellant Rocket Engines* (AIAA, 2012).
3. D. Glover, NASA Cryogenic fluid management space experiment efforts, 1960-1990 (Report NASA-TM-103752, NASA, 1991).
4. E. Lakdawalla, China lands on the Moon. *Nat. Geosci.* **7**, 81 (2014).
5. A. Pasini, L. Torre, G. Pace, D. Valentini, L. d'Agostino, Pulsed chemical rocket with green high performance propellants, in 49th AIAA/ASME/SAE/ASEE Joint Propulsion Conference, San Jose, CA, 14 to 17 July 2013.
6. J. A. Mahn, Getting to necessary and sufficient-developing accident scenarios for risk assessment (Report SAND-96-0885C, Sandia National Laboratory, 1996).
7. L. T. De Luca, *Chemical Rocket Propulsion* (Springer Nature, 2017).
8. Q. Zhang, J. M. Shreeve, Energetic ionic liquids as explosives and propellant fuels: A new journey of ionic liquid chemistry. *Chem. Rev.* **114**, 10527–10574 (2014).
9. L.-L. Dong, L. He, H. Liu, G.-H. Tao, F.-D. Nie, M. Huang, C.-W. Hu, Nitrogen-rich energetic ionic liquids based on the *N*, *N*-bis (1*H*-tetrazol-5-yl) amine anion-syntheses, structures, and properties. *Eur. J. Inorg. Chem.* **2013**, 5009–5019 (2013).
10. S. Schneider, T. Hawkins, M. Rosander, G. Vaghjiani, S. Chambreau, G. Drake, Ionic liquids as hypergolic fuels. *Energy Fuels* **22**, 2871–2872 (2008).
11. H. Gao, Y.-H. Joo, B. Twamley, Z. Zhou, J. M. Shreeve, Hypergolic ionic liquids with the 2,2-dialkyltriazanium cation. *Angew. Chem. Int. Ed.* **48**, 2792–2795 (2009).
12. L. He, G.-H. Tao, D. A. Parrish, J. M. Shreeve, Nitrocyanamide-based ionic liquids and their potential applications as hypergolic fuels. *Chem. Eur. J.* **16**, 5736–5743 (2010).
13. J. Giles, Green explosives: Collateral damage. *Nature* **427**, 580–581 (2004).
14. P. D. McCrary, P. A. Beasley, S. A. Alaniz, C. S. Griggs, R. M. Frazier, R. D. Rogers, Graphene and graphene oxide can "lubricate" ionic liquids based on specific surface interactions leading to improved low-temperature hypergolic performance. *Angew. Chem. Int. Ed.* **51**, 9784–9787 (2012).
15. P. D. McCrary, P. A. Beasley, O. A. Cojocaru, S. Schneider, T. W. Hawkins, J. P. L. Perez, B. W. McMahon, M. Pfeil, J. A. Boatz, S. L. Anderson, S. F. Son, R. D. Rogers, Hypergolic ionic liquids to mill, suspend, and ignite boron nanoparticles. *Chem. Commun.* **48**, 4311–4313 (2012).
16. G. Steinhauser, "Green" pyrotechnics: A chemists' challenge. *Angew. Chem. Int. Ed.* **47**, 3330–3347 (2008).
17. H. I. Schlesinger, H. C. Brown, A. E. Finholt, J. R. Gilbreath, H. R. Hoekstra, E. K. Hyde, Sodium borohydride, its hydrolysis and its use as a reducing agent and in the generation of hydrogen. *J. Am. Chem. Soc.* **75**, 215–219 (1953).
18. P. G. Boyd, Y. Lee, B. Smit, Computational development of the nanoporous materials genome. *Nat. Rev. Mater.* **2**, 17037 (2017).
19. S. Curtarolo, G. L. W. Hart, M. B. Nardelli, N. Mingo, S. Sanvito, O. Levy, The high-throughput highway to computational materials design. *Nat. Mater.* **12**, 191–201 (2013).
20. C. E. Wilmer, M. Leaf, C. Y. Lee, O. K. Farha, B. G. Hauser, J. T. Hupp, R. Q. Snurr, Large-scale screening of hypothetical metal-organic frameworks. *Nat. Chem.* **4**, 83–89 (2012).
21. H. H. Koelle, The influence of lunar propellant production on the cost-effectiveness of cislunar transportation systems (Report 19930004795, NASA, 1992).
22. S. Berg, J. Rovey, Dual-mode propellant properties and performance analysis of energetic ionic liquids, in 50th AIAA Aerospace Sciences Meeting including the New Horizons Forum and Aerospace Exposition, Nashville, Tennessee, 9 to 12 January 2012.
23. T. Liu, X. Qi, S. Huang, L. Jiang, J. Li, C. Tang, Q. Zhang, Exploiting hydrophobic borohydride-rich ionic liquids as faster-igniting rocket fuels. *Chem. Commun.* **52**, 2031–2034 (2016).
24. K. Anflo, T.-A. Grönland, Towards green propulsion for spacecraft with ADN-based monopropellants, in 38th AIAA/ASME/SAE/ASEE Joint Propulsion Conference & Exhibit, Indianapolis, Indiana, 7 to 10 July 2002.

25. T. Welton, Room-temperature ionic liquids. solvents for synthesis and catalysis. *Chem. Rev.* **99**, 2017–2084 (1999).
26. H. Gao, J. M. Shreeve, Azole-based energetic salts. *Chem. Rev.* **111**, 7377–7436 (2011).
27. A. J. Alfano, J. D. Mills, G. L. Vaghjiani, Highly accurate ignition delay apparatus for hypergolic fuel research. *Rev. Sci. Instrum.* **77**, 045109 (2006).
28. L. R. Rapp, M. P. Strier, The effect of chemical structure on the hypergolic ignition of amine fuels. *J. Jet Prop.* **27**, 401–404 (1957).
29. L. Zhang, L. He, C.-B. Hong, S. Qin, G.-H. Tao, Brønsted acidity of bio-protic ionic liquids: The acidic scale of [AA]X amino acid ionic liquids. *Green Chem.* **17**, 5154–5163 (2015).
30. M. T. Clough, C. R. Crick, J. Gräsvik, P. A. Hunt, H. Niedermeyer, T. Welton, O. P. Whitaker, A physicochemical investigation of ionic liquid mixtures. *Chem. Sci.* **6**, 1101–1114 (2015).
31. I. Frank, A. Hammerl, T. M. Klapötke, C. Nonnenberg, H. Zewen, Processes during the hypergolic ignition between monomethylhydrazine (MMH) and dinitrogen tetroxide (N_2O_4) in rocket engines. *Propell. Explos. Pyrot.* **30**, 44–52 (2005).
32. L. T. De Luca, T. Shimada, V. P. Sinditskii, M. Calabro, *Chemical Rocket Propulsion: A Comprehensive Survey of Energetic Materials* (Springer, 2016).
33. G.-H. Tao, D. A. Parrish, J. M. Shreeve, Nitrogen-rich 5-(1-methylhydrazinyl) tetrazole and its copper and silver complexes. *Inorg. Chem.* **51**, 5305–5312 (2012).
34. G.-H. Tao, M. Tang, L. He, S.-P. Ji, F.-D. Nie, M. Huang, Synthesis, structure and property of 5-aminotetrazolate room-temperature ionic liquids. *Eur. J. Inorg. Chem.* **2012**, 3070–3078 (2012).
35. C. M. Nichols, Z.-C. Wang, Z. Yang, W. C. Lineberger, V. M. Bierbaum, Experimental and theoretical studies of the reactivity and thermochemistry of dicyanamide: $N(CN)_2^-$. *J. Phys. Chem. A* **120**, 992–999 (2016).
36. M. J. McQuaid, Computationally Based Measures of Amine Azide Basicity and Their Correlation with Hypergolic Ignition Delays (Report No. ARL-TR-3122, Army Research Lab, Aberdeen Proving Ground 2003).
37. T. Litzinger, S. Iyer, Hypergolic reaction of dicyanamide-based fuels with nitric acid. *Energy Fuels* **25**, 72–76 (2011).
38. H. Kubinski, G. E. Gutzke, Z. O. Kubinski, DNA-cell-binding (DCB) assay for suspected carcinogens and mutagens. *Mutat. Res.* **89**, 95–136 (1981).
39. K. M. Docherty, C. F. Kulpa Jr., Toxicity and antimicrobial activity of imidazolium and pyridinium ionic liquids. *Green Chem.* **7**, 185–189 (2005).
40. M. J. Casiano, J. R. Hulka, V. Yang, Liquid-propellant rocket engine throttling: A comprehensive review. *J. Propuls. Power* **26**, 897–923 (2010).
41. M. J. Frisch, G. W. Trucks, H. B. Schlegel, G. E. Scuseria, M. A. Robb, J. R. Cheeseman, G. Scalmani, V. Barone, B. Mennucci, G. A. Petersson, H. Nakatsuji, M. Caricato, X. Li, H. P. Hratchian, A. F. Izmaylov, J. Bloino, G. Zheng, J. L. Sonnenberg, M. Hada, M. Ehara, K. Toyota, R. Fukuda, J. Hasegawa, M. Ishida, T. Nakajima, Y. Honda, O. Kitao, H. Nakai, T. Vreven, J. A. Montgomery Jr., J. E. Peralta, F. Ogliaro, M. Bearpark, J. J. Heyd, E. Brothers, K. N. Kudin, V. N. Staroverov, R. Kobayashi, J. Normand, K. Raghavachari, A. Rendell, J. C. Burant, S. S. Iyengar, J. Tomasi, M. Cossi, N. Rega, J. M. Millam, M. Klene, J. E. Knox, J. B. Cross, V. Bakken, C. Adamo, J. Jaramillo, R. Gomperts, R. E. Stratmann, O. Yazyev, A. J. Austin, R. Cammi, C. Pomelli, J. W. Ochterski, R. L. Martin, K. Morokuma, V. G. Zakrzewski, G. A. Voth, P. Salvador, J. J. Dannenberg, S. Dapprich, A. D. Daniels, O. Farkas, J. B. Foresman, J. V. Ortiz, J. Cioslowski, D. J. Fox, Gaussian 09, Revision A.01 (Gaussian Inc., 2009).
42. R. G. Parr, *Density Functional Theory of Atoms and Molecules* (Oxford Univ. Press, 1989).
43. A. D. Becke, Density functional thermochemistry. III. The role of exact exchange. *J. Chem. Phys.* **98**, 5648–5652 (1993).
44. T. Lu, F. Chen, Quantitative analysis of molecular surface based on improved Marching Tetrahedra algorithm. *J. Mol. Graph. Model.* **38**, 314–323 (2012).

Acknowledgments: We gratefully acknowledge the test platform of the specialized laboratory, College of Chemistry, Sichuan University and the Analytical and Testing Center of the Sichuan University for instrumental measurements. We also acknowledge X.-P. Li (Chengdu ST. Science and Technology Co. Ltd.) for the use of high-speed camera and Y. An (Hangzhou Netease Game Co. Ltd.) for the software support. **Funding:** This work was supported by the National Natural Science Foundation of China (nos. 21876120, 21973062, and 21303108), the Fundamental Research Funds for the Central Universities (20826041D4117), the China Scholarship Council, and the Academy-School Cooperation Project (S18H321-Q). **Author contributions:** W.-L.Y., L.Z., G.-H.T., L.H., and J.M.S. designed the studies and wrote the paper. W.-L.Y., L.Z., S.-L.W., Q.-H.Z., G.-H.Z., and Y.W. conducted the experiments. W.-L.Y., L.Z., and L.H. carried out the data analyses. Z.Z., Y.X., S.Q., and G.-H.T. provided the technical support throughout. **Competing interests:** The authors declare that they have no competing interests. **Data and materials availability:** All data needed to evaluate the conclusions in the paper are present in the paper and/or the Supplementary Materials. Additional data related to this paper may be requested from the authors.

Submitted 21 February 2020
Accepted 21 October 2020
Published 4 December 2020
10.1126/sciadv.abb1899

Citation: W.-L. Yuan, L. Zhang, G.-H. Tao, S.-L. Wang, Y. Wang, Q.-H. Zhu, G.-H. Zhang, Z. Zhang, Y. Xue, S. Qin, L. He, J. M. Shreeve, Designing high-performance hypergolic propellants based on materials genome. *Sci. Adv.* **6**, eabb1899 (2020).